Catalysis Today 149 (2010) 69–75

Contents lists available at ScienceDirect

Catalysis Today

journal homepage: www.elsevier.com/locate/cattod

Zeolite beta synthesized with acid-treated metakaolin and its application in diesel hydrodesulfurization

Guofu Wan [a,b], Aijun Duan [a,*], Ying Zhang [c], Zhen Zhao [a,*], Guiyuan Jiang [a], Dengqian Zhang [a], Zhenyong Gao [a]

[a] State Key Laboratory of Heavy Oil Processing, China University of Petroleum, Beijing 102249, PR China
[b] College of Mechanical and Energy Engineering, Jiangsu Polytechnic University, Changzhou 213016, PR China
[c] Department of Materials Science and Engineering, University of Petroleum, Beijing 102249, PR China

ARTICLE INFO

Keywords:
Hydrodesufurization
FCC diesel
Zeolite beta
Kaolin
In situ synthesized method

ABSTRACT

A new type of zeolite beta (denoted as MB) with multi-pore system was synthesized by using in situ synthesized method from kaolin mineral in this study. NiW/Al_2O_3–MB and NiW/TiO_2–Al_2O_3–MB catalysts were prepared and the hydrodesulfurization (HDS) activities of these catalysts were evaluated with FCC diesel feed. The samples were characterized by N_2 physisorption, XRD, SEM, TPR, FT-IR spectroscopy of pyridine adsorption, HRTEM and XPS techniques. The HDS results showed that the MB-containing catalyst exhibited much higher HDS conversion (98.7%) than that of NiW/γ-Al_2O_3 (97.5%). The incorporation of TiO_2 into the composite supports further increased the HDS conversion (99.3%) of NiW/TiO_2–Al_2O_3–MB. The higher HDS activity was mainly associated with the appropriate ratio of B/L (Brönsted acid/Lewis acid) and the enhanced hydrogenation activity.

1. Introduction

Clean fuel research has been becoming an important subject due to increasing awareness of the impact of environmental pollution from automobile exhausts. In view of diesel fuels as an important transportation power, the reduction of the sulfur content in diesel is one of the primary regulations, and the sulfur content is expected to be lowered to 10–50 ppm level in most of the developed countries and developing countries by the end of this decade [1]. The hydrodesulfurization technologies have become the effective choices to meet the ultra low-sulfur fuel specifications, whereas the conventional hydrodesulfurization (HDS) processes cannot currently produce ultra low-sulfur diesel fuels. The essential approaches are to design and develop more active HDS catalysts.

Traditional HDS catalysts were mainly alumina-supported Mo (W) sulfides coacted by Ni(Co) promoter. Studies have shown that the catalyst supports could effectively promote the dispersion of the active components and thus alter the catalytic functionalities through metal–support interaction (MSI) [2]. Among the various research works on HDS catalyst supports, more and more attention was paid to composite supports, particularly the combination of TiO_2 and Al_2O_3 because of the increased reducibility and sulfurability of Ti-containing catalysts, which were related to the fact that the redox processes of the active phases (Mo species) were facilitated by the semiconductor characteristics of TiO_2 compared with the pure insulating Al_2O_3 material [3–5].

Deep HDS requires sulfur removal from highly hindered compounds like 4,6-DMDBT, which cannot be removed the sulfur through the direct desulfurization route (DDS) due to the restriction of the side-chain alkyls. It was well known that the sulfur removal of DBT was converted predominantly via the DDS pathway, whereas 4,6-DMDBT reacted mainly via the hydrogenation (HYD) pathway. In order to diminish the steric hindrance of refractory compounds such as 4,6-DMDBT, two approaches have been proposed. The first method was the improvement of the hydrogenation activity of the hydrotreating catalysts since the HYD pathway was not hindered by the methyl groups in 4,6-DMDBT [6], the other method involved diminishing the steric hindrance by acid-catalyzed reactions namely isomerization, demethylation or transalkylation, etc. [6–8].

Previous studies had revealed that the addition of acidic zeolites into the traditional alumina-supported hydrotreating catalysts could greatly enhance their hydrodesulfurization activities [9,10]. It had been reported that mixed supports containing zeolites and alumina for NiMoS showed high HDS activity and resistivity against H_2S [11]. The introduction of zeolite into the alumina

* Corresponding authors. Tel.: +86 10 89731586.
E-mail addresses: duanaijun@cup.edu.cn, wanguofu001@163.com (A. Duan), zhenzhao@cup.edu.cn (Z. Zhao).

0920-5861/$ – see front matter © 2009 Elsevier B.V. All rights reserved.
doi:10.1016/j.cattod.2009.07.098

enhanced the hydrogenation of neighbored aromatic rings, isomerization and disproportionation into more reactive derivatives [6,12]. Among the acidic components, zeolite Y was the leading actor in most studied for its high acidity in many catalysis processes [8,13]. Another acidic zeolite beta which was similar to zeolite Y, had a 3D porous structure and a higher SiO_2/Al_2O_3 ratio, furthermore, zeolite beta showed tunable and suitable acidity, higher hydroisomerization activity, lower hydrogen-transfer capacity and lower catalyst deactivation [14,15]. These characteristics made zeolite beta more attractive in the employment for deep HDS and resisted catalyst deactivation. Previous studies mainly focused on the application of zeolites especially Y and beta in the hydrocracking of heavy oil [12,15,16]. In the studies of hydrotreating of FCC diesel, scarce research [17] could be found using zeolite beta as acidic components of the catalyst.

The main objective of this study is to investigate the HDS performance of the NiW catalysts using Al_2O_3–MB and TiO_2–Al_2O_3–MB composite as supports and FCC diesel as a feedstock. Herein, MB used in the work is a new type of zeolite beta with multi-pore system prepared from kaolin mineral via in situ synthesized method. A high deep HDS conversion (above 99.3%) has been achieved over the NiW catalysts using a composite of alumina, titania and zeolite as the support.

2. Experimental

2.1. Preparation of zeolite beta (MB), Al_2O_3–MB and TiO_2–Al_2O_3–MB composite supports

MB was prepared by in situ crystallization method from kaolin according to our previous work [18]. The Suzhou kaolin mineral was firstly calcined at 720 °C for 4 h and then was treated with 20 wt% HCl solution at 94 °C under reflux conditions. The solid with SiO_2/Al_2O_3 molar ratio of 88 was obtained. In a typical process, 16.0 g of HCl-treated solid was added to a mixture solution composed of 3.2 g NaOH and 46.4 g of TEAOH aqueous solution (15.9 wt%) under stirring. Then the resulted mixture with a molar ratio of $Na_2O:Al_2O_3:SiO_2$:TEAOH:H_2O at 4.5:1.0:88.0:6.0:756.8 was transferred into a 200 ml autoclave and placed at 170 °C for 30 h. After crystallization, the solid product was filtered, washed, dried and calcined at 550 °C for 6 h. The protonated form (denoted as H-MB) was obtained by calcining the NH_4^+ form of beta zeolite at 500 °C for 5 h. Then H-MB powder was dispersed uniformly in deionized water, the obtained suspension was added dropwise into the pseudoboehmite sol. Subsequently, a part of the sol mixture was transferred and stirred vigorously in a water bath at 75 °C until the mixture became a viscous paste; and titanium-sol (made from the tetra-*n*-butyl-titanate, ethanol, nitric acid and deionized distilled water with the molar ratio of 1:15:0.3:3) was dripped into another part sol under the drastic stirring condition to form the gel and also stirred vigorously in a water bath at 75 °C until the mixture became viscous paste. Then the gels obtained followed by drying at 120 °C for 4 h and calcination at 550 °C for 4 h. The obtained supports were designed as Al_2O_3–MB (Al_2O_3 and H-MB with the weight ratio of 2.1:1) and TiO_2–Al_2O_3–MB (TiO_2, Al_2O_3 and H-MB with the weight ratio of 0.16:2.1:1), respectively. For comparison, TiO_2–Al_2O_3–B (zeolite beta, SiO_2/Al_2O_3 = 30, supplied by Nankai University Catalyst Co., China) also was prepared according to the preparation method for TiO_2–Al_2O_3–MB. These supports were ready for metal impregnation.

2.2. Preparation of supported NiW catalysts

The NiW catalysts were prepared using co-impregnation and incipient-wetness impregnation method with an aqueous solution of the appropriate amounts of ammonium metatungstate hydrate [$(NH_4)_6W_{12}O_{39}\cdot H_2O$] and nickel nitrate hexahydrate [$Ni(NO_3)_2\cdot 6H_2O$]. After impregnation, the impregnated precursors were dispersed in an ultra-sonic unit for 30 min. Then the prepared samples were dried at 110 °C for 12 h, and calcined at 500 °C for 4 h. All the catalysts were prepared with the constant amounts of W and Ni (corresponding to 27 wt% of WO_3 and 3.5 wt% of NiO, respectively).

2.3. Catalyst characterization

Porosity and surface area measurements of samples were performed on a Micromeritics ASAP 2020 automated gas adsorption system. All the samples were outgassed at 350 °C under vacuum prior to N_2 adsorption at −196 °C. Mercury porosimetry experiments were carried out on a Micromeritics AutoPoreIV 9500 apparatus in the pressure range 0–30,000 psia. SEM observations were carried out using a Cambridge S-360 electron microscope. The nature of acid sites of the catalysts was determined by pyridine-adsorbed Fourier transformed infrared (Py-FTIR) spectrum experiments conducted on a MAGNAIR 560 FTIR instrument (Nicolet Co., America) with a resolution of 1 cm^{-1}. The samples were dehydrated at 500 °C for 5 h under a vacuum of 1.33×10^{-3} Pa, following by the adsorption of purified pyridine vapor at room temperature for 20 min. Then, the system was evacuated at different temperatures and pyridine-adsorbed IR spectra were recorded. The Brönsted and Lewis acid sites could be distinguished by the bands of chemisorbed pyridine at ~1540 cm^{-1} and coordinative bonded pyridine at ~1450 cm^{-1}, respectively. X-ray powder diffraction (XRD) profiles were recorded in an XRD-6000 diffractometer using Cu Kα radiation under 40 kV, 30 mA, scan range from 5° to 80° at a rate of 4° min^{-1}. Afterwards, H_2-TPR was carried out using 10% hydrogen in argon at a constant flow rate of 40 mL min^{-1}, from room temperature to 1000 °C, at a heating rate of 10 °C min^{-1}. The HRTEM measurements of the sulfided catalysts were carried out on a Tecnai G2 F20 transmission electron microscope (Philips) operated at an accelerating voltage of 200 kV. The catalysts were sulfided with a 2 wt% CS_2/cyclohexane mixture at 320 °C for 6 h and placed in cyclohexane before measurement. The XPS spectra of the samples were taken on an ESCA Lab 220i-XL electron spectrometer (VG) using 300 W Mg Kα radiation. The binding energies were corrected by using the C1s peak at 284.6 eV as a reference.

2.4. Catalytic activity measurement

Catalytic performance was evaluated in a high-pressure fixed-bed reactor with 2 g of catalyst (grain size of 0.3–0.5 mm). All catalysts were presulfided for 6 h with a 2 wt% CS_2–cyclohexane mixture under the conditions of LHSV (Liquid Hourly Space Velocity) of 1.0 h^{-1}, temperature of 320 °C, total pressure of 4 MPa and a H_2/cyclohexane ratio of 600 mL mL^{-1}. Hydrodesulfurization tests of diesel were carried out under the conditions of 350 °C, 5.0 MPa, 600 mL mL^{-1} and 1.0 h^{-1}. Catalytic activities were measured at steady states after 13 h on-stream. The typical properties of diesel feed are listed in Table 1.

The total sulfur content in the feed and products was measured by using a LC-4 coulometric sulfur analyzer system. The distributions of sulfur species in feed and products were identified by Finnigan Trace GC/MS with a Trace Ultra gas chromatograph using a HP-5MS (30 × 0.25 × 0.25) capillary column and a pulsed flame photometric detector (PFPD). The catalytic activity under investigation was estimated by the HDS efficiency.

Table 1
The typical properties of diesel feedstock.

Properties	Data
Density @ 20 °C/g cm^{-3}	0.8566
Sulfur/ppm	1300
Distillation	
IBP	172
10%	220
30%	255
50%	287
70%	316
95%	362
FBP	451

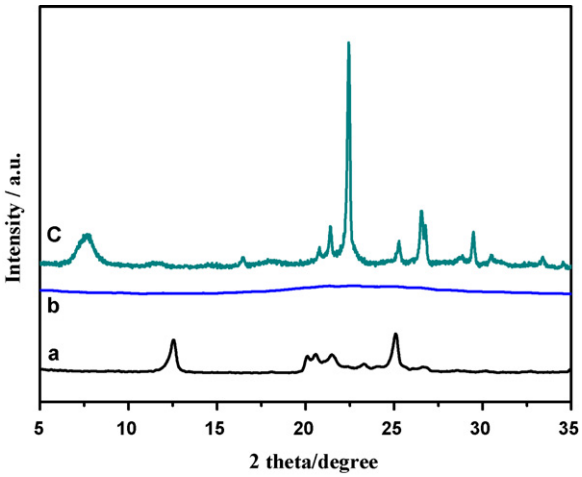

Fig. 1. The XRD patterns of (a) kaolin, (b) acid-treated metakaolin and (c) as-synthesized MB.

3. Results and discussion

3.1. Characterization of MB

The XRD patterns of kaolin, acid-treated metakaolin and as-synthesized MB are shown in Fig. 1. It can be seen that the kaolin sample (Fig. 1a) shows two intense diffraction peaks at $2\theta = 12.5^\circ$ and 25.2° and a hump between $2\theta = 19.8$–22° of kaolinite. The acid-treated metakaolin shows amorphous patterns (as shown in Fig. 1b), and MB synthesized from acid-treated metakaolin shows an XRD pattern (as shown in Fig. 1c) with new and very intense peaks at $2\theta = 7.5^\circ$, 22.5° and 26.5° that closely match the characteristic peaks of zeolite beta.

Table 2
The typical properties of starting materials and MB product.

Samples	S_{BET}/m^2 g^{-1}	Pore volume/cm^3 g^{-1}
Kaolin	28.5	0.28
Acid-treated metakaolin	297.0	0.48
MB	550.6	0.30

It can be seen, from Fig. 2C, as-synthesized zeolite MB is present as loose aggregates of particles composed of smaller cubelike crystals (around 500–1000 nm diameter) with smooth surface unlike kaolin (in Fig. 2A) and the acid-treated metakaolin (in Fig. 2B) which shows 'spongy' particles.

It is clear that MB possesses much higher specific surface area than the starting materials of kaolin (as shown in Table 2). Notably, unlike the conventional zeolite beta only having microporous structure, MB prepared from the acid-treated metakaolin not only possesses micropores, but also gives narrowly distributed mesopores around 3.6 nm (Fig. 3A) and macropores distributed around 180 nm (Fig. 3B); while H-MB shows the similar distributions of mesopores around 3.8 nm (Fig. 3A) and macropores around 151 nm (Fig. 3B). From Fig. 3A and B, it can be seen that both the kaolin and the acid-treated metakaolin possess 3.7–4 nm mesopores and 30–40 nm macropores. It is also be seen that after the HCl treatment, the mesopores at around 4 nm of the acid-treated metakaolin grow larger and obvious than those of kaolin, and the macropores diameters distribution of the kaolin shift from 40 to 30 nm, thus it is concluded that the mesopores or macropores in the MB products are supposed to be inherited from the kaolin starting materials and the changes in pore structure are due to the aluminium of metakaolin leached out by HCl treatment. The multi-pore system characters of MB and H-MB make them the promising support candidates for acid-catalyzed reaction of large molecules such as diesel HDS.

3.2. Characterization of NiW catalysts

3.2.1. XRD analysis

The XRD profiles of the oxidic NiW catalysts are shown in Fig. 4. The characteristic diffraction peaks of γ-Al_2O_3 appears in all oxide catalysts. The characteristic diffraction peaks of zeolite beta ($2\theta = 22.4^\circ$ and 7°) were detected in the zeolite beta-containing catalysts. Compared with NiW/Al_2O_3, in NiW/Al_2O_3–MB and NiW/TiO_2–Al_2O_3–MB catalysts after the incorporation of H-MB, the diffraction peak intensities of γ-Al_2O_3 were decreased. No detectable characteristic peak of WO_3, NiO or $NiAl_2O_4$ crystal phases was found in the oxide catalysts. This means that WO_3 and NiO are high dispersed on the support surface or their crystallite sizes are smaller than 4 nm.

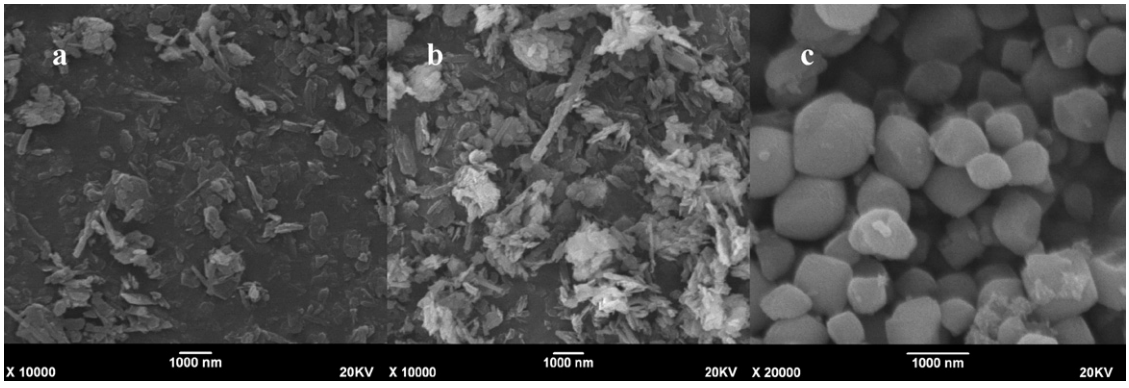

Fig. 2. SEM images of (A) kaolin, (B) acid-treated metakaolin and (C) as-synthesized MB.

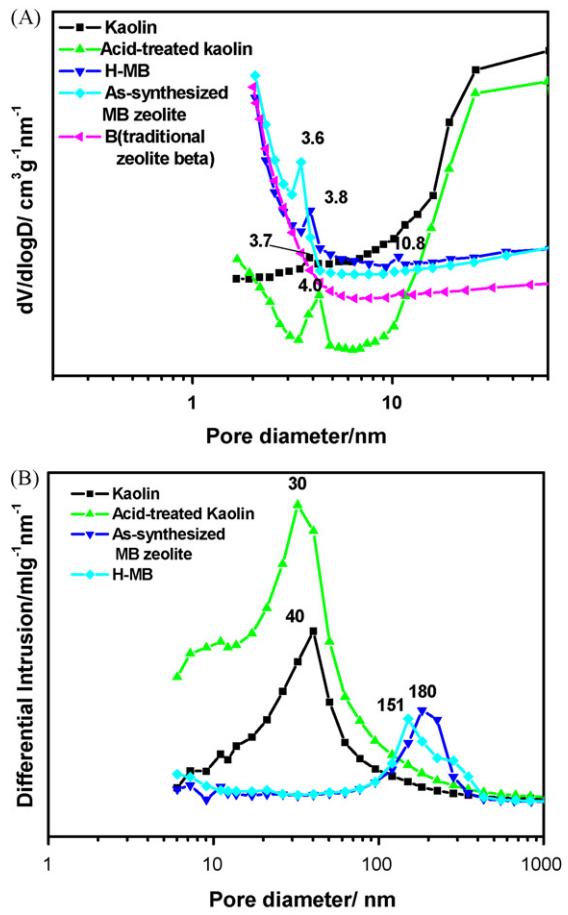

Fig. 3. The pore size distribution curves of starting materials and MB products (A) determined by N_2 adsorption method and (B) determined by Mercury porosimetry method.

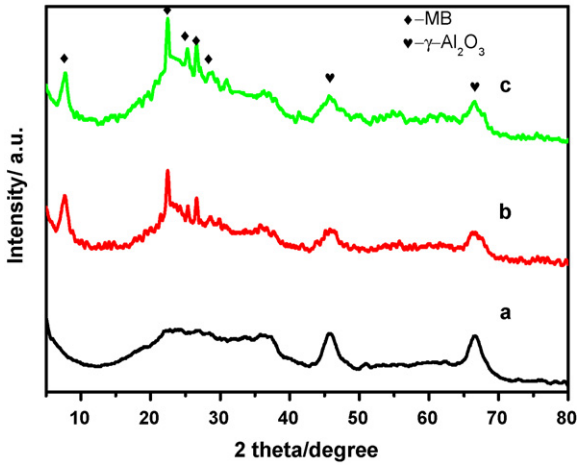

Fig. 4. The XRD patterns of (a) NiW/Al_2O_3, (b) NiW/Al_2O_3–MB and (c) NiW/TiO_2–Al_2O_3–MB.

3.2.2. Specific surface area and pore volume

Textural properties of the catalysts are listed in Table 3. The specific surface areas of NiW catalysts increased whereas the average diameters decreased after the H-MB were introduced to the catalyst. However, the addition of H-MB slightly changed the pore volumes. The NiW/TiO_2–Al_2O_3–MB showed a smaller specific surface area than NiW/Al_2O_3–MB due to the addition of TiO_2 with low surface area. The pore size distributions unambiguously

Table 3
Textural properties of the NiW catalysts.

Samples	$S_{BET}/m^2\,g^{-1}$	Pore volume/$cm^3\,g^{-1}$	Average diameter/nm
Al_2O_3	203.0	0.31	5.4
NiW/Al_2O_3	126.8	0.21	5.3
NiW/Al_2O_3–MB	194.1	0.22	3.7
NiW/TiO_2–Al_2O_3–MB	172.8	0.20	3.8
NiW/TiO_2–Al_2O_3–B	154.3	0.16	3.8

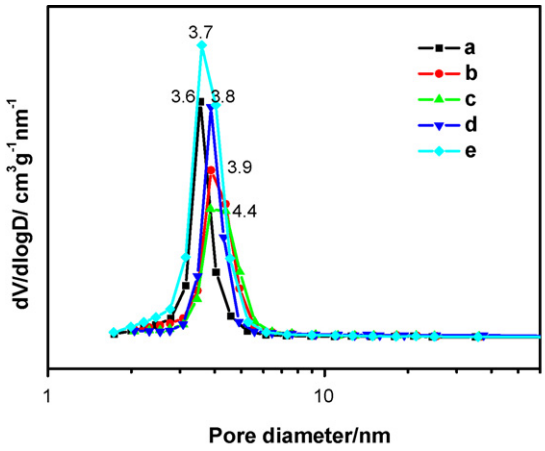

Fig. 5. The pore size distributions of (a) NiW/Al_2O_3, (b) NiW/Al_2O_3–MB, (c) NiW/TiO_2–Al_2O_3–MB, (d) NiW/TiO_2–Al_2O_3–B and (e) Al_2O_3.

demonstrated the preservation of the mesoporous structure in these catalysts. Meanwhile, pore sizes of MB-containing catalysts as well as Al_2O_3 and NiW/TiO_2–Al_2O_3–B catalyst were centered around 3.5–4.5 nm (in Fig. 5).

3.2.3. TPR analysis

The TPR profiles of the NiW oxide catalysts, including NiO/Al_2O_3, WO_3/Al_2O_3, NiW/Al_2O_3, NiW/Al_2O_3–MB, NiW/TiO_2–Al_2O_3–MB, WO_3 and NiO are shown in Fig. 6. The TPR profile of bulk WO_3 exhibited three main peaks with maxima at 739, 782 and 951 °C. The two higher temperature peaks at 782 and 951 °C were associated with the reduction of W(VI) species in the tetrahedral coordination [19], while the peak at lower temperature (739 °C) was correlated with the reduction of polymeric octahedral W species or the supported WO_3 crystallites [20]. These peaks might be assigned to the three-step reductions of WO_3 to W(0)

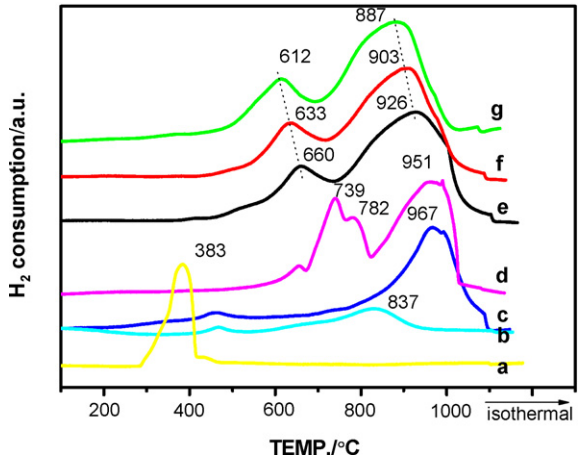

Fig. 6. The H_2-TPR profiles of (a) NiO, (b) NiO/Al_2O_3, (c) WO_3/Al_2O_3, (d) WO_3, (e) NiW/Al_2O_3, (f) NiW/Al_2O_3–MB and (g) NiW/TiO_2–Al_2O_3–MB.

Table 4
Amounts of B and L acids determined by FT-IR of pyridine adsorption for NiW catalysts at different degassed temperatures.

Samples	Amount of acid sites (μmol g^{-1}) (200 °C)				Amount of acid sites (μmol g^{-1}) (350 °C)			
	L	B	B+L	B/L	L	B	B+L	B/L
NiW/Al_2O_3	620.24	45.76	666.00	0.074	292.86	37.46	340.32	0.123
NiW/Al_2O_3–MB	397.62	59.32	456.94	0.149	170.24	27.12	197.36	0.159
NiW/TiO_2–Al_2O_3–MB	280.04	27.39	307.43	0.098	160.37	21.65	182.02	0.135

[WO_3(VI) → $WO_{2.9}$(V,VI) → WO_2(IV) → W(0)] according to the literatures [19,21]. The profile of bulk NiO showed only a peak at 383 °C in accordance with the results of Sheffer et al. [22]. The TPR profile of all NiW catalysts showed two principal reduction peaks at 600–800 and 800–1000 °C regions, respectively. By resemblance to W/Al_2O_3 and Ni/Al_2O_3, the high temperature broad peak could be assigned to the superimposed reduction of tetrahedrally coordinated W species and Ni species, and the low temperature peak could be assigned to the reduction of polymeric octahedral W species or WO_3 crystallites. Compared with the WO_3/Al_2O_3 sample, the position of high temperature peak exhibited an obvious shift to lower temperature for all NiW catalysts, indicating that some of the W species were easier to be reduced by the presence of Ni species. This phenomenon was in accordance with the known promoter effect of nickel species on the reduction of tungsten observed by Sheffer et al. [22] in NiW/Al_2O_3 catalysts. Moreover, after incorporating H-MB into the support, two intense peaks of the NiW/Al_2O_3–MB catalyst shifted toward rather lower temperature, which demonstrated that metal oxide species of WO_3 and NiO had weaker interaction with the Al_2O_3–MB support than that with Al_2O_3 support. Especially, when TiO_2 and H-MB were introduced simultaneously to the catalyst, the peak temperatures further decreased. It may be due to the decrease of the reactive surface hydroxyl groups of alumina caused by the addition of TiO_2. The modification of the surface of alumina with TiO_2 can constrain the formation of tetrahedral W oxide species which are difficultly reduced, resulting in an increase in the content of octahedral W oxide species which are easily reduced [23]. It could be concluded that the incorporation of MB and/or TiO_2 could play a beneficial role in adjusting the metal–support interactions and caused easier reductions of nickel and tungsten. Similar results had been found in the work reported by Solís et al. [24].

3.2.4. Adsorbed-pyridine FT-IR analysis

The Brönsted and Lewis acidities of the samples were determined by FT-IR spectroscopy of pyridine adsorption [25,26]. Table 4 shows the adsorption amounts of pyridine which were degassed at 200 and 350 °C. The adsorption amounts of pyridine degassed at 200 °C, correspond to the total acid amounts, while the adsorption amounts of pyridine degassed at relatively high temperature of 350 °C, correspond to the acid amounts of strong and medium strength acid. After metal component impregnations, all NiW catalysts showed the presence of both L acid sites and B acid sites. For NiW catalysts, compared with the acid amounts of NiW/Al_2O_3, the incorporation of H-MB led mainly to a decrease of the total amounts of B and L acid sites but an increase of B acid proportion or the ratio of B/L in both weak acid case (200 °C) and strong acid case (350 °C). Furthermore, when TiO_2 accompanied with H-MB was introduced to the catalyst, NiW/TiO_2–Al_2O_3–MB showed the lower amounts of B acid or L acid than those of other two catalysts, but the ratio of B/L, i.e., the proportion of B acid, was still higher than that of NiW/Al_2O_3. The incorporation of H-MB and/or TiO_2 to the NiW catalyst not only modulated the total amounts of acidic sites but also regulated the acid types, i.e., the ratio of B/L. The changes of acid properties would have an important effect on the catalytic HDS activity of the catalyst.

3.2.5. HRTEM analysis

The representative HRTEM images of the sulfided NiW catalysts are shown in Fig. 7A–C. The dark fringes in the images were WS_2 crystallites. The particles of the promoter Ni sulfide on the catalysts were too small to be visualized in the HRTEM images, because they were usually with the size of about 0.5 nm and lay in the WS_2 slabs [27,28]. NiW/Al_2O_3 (in Fig. 7A) catalyst showed mostly single-layer slabs and small amounts of three-dimensional structures having two or three layers, whereas NiW/Al_2O_3–MB (in Fig. 7B) and NiW/TiO_2–Al_2O_3–MB (in Fig. 7C) mostly exhibited multilayered WS_2 slabs.

To quantitatively compare the lengths and stacking numbers of the WS_2 slabs on the three catalysts, statistical analyses were made based on at least 15 images including 240–280 slabs taken from the different parts of each catalyst as shown in Fig. 8. For NiW/Al_2O_3 catalyst, the average slab length L was equal to 4.1 nm, and the average layer number N was equal to 1.8. While for NiW/Al_2O_3–MB catalyst, the average length L of WS_2 slabs increased to 9.4 nm, and the average layer number N increased to 3.1, and for NiW/TiO_2–Al_2O_3–MB case, the average length L of WS_2 slabs was 9.0 nm, and the average layer number N was 2.6. Compared with NiW/Al_2O_3, MB-containing catalysts exhibited a broad slab length distribution and a higher layer number. This is probably related to the different textures of the supports, due to the addition of MB. Higher WS_2 stacking degree in sulfided NiW/Al_2O_3–MB and NiW/

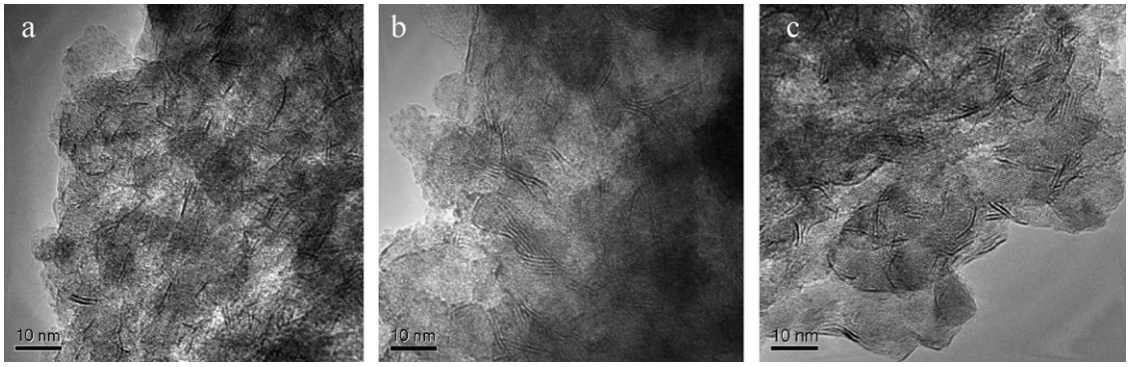

Fig. 7. The HRTEM images of the sulfided (A) NiW/Al_2O_3, (B) NiW/Al_2O_3–MB and (C) NiW/TiO_2–Al_2O_3–MB.

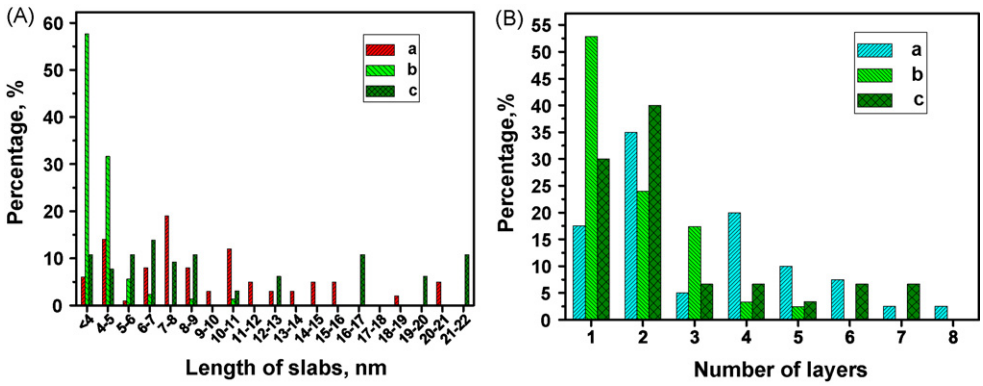

Fig. 8. Slab length (A) and stacking layer number (B) distributions of the WS_2 slabs on the sulfided (a) NiW/Al_2O_3–MB, (b) NiW/Al_2O_3 and (c) NiW/TiO_2–Al_2O_3–MB.

TiO_2–Al_2O_3–MB might be due to the lower metal–support interaction, which would lead to the formation of type-II WS_2 phase. The longer WS_2 slab lengths of sulfided NiW/Al_2O_3–MB and NiW/TiO_2–Al_2O_3–MB catalysts might result from the low dispersion in the oxide precursor. Meanwhile, the morphology of WS_2 structures on sulfided NiW/Al_2O_3–MB and NiW/TiO_2–Al_2O_3–MB showed more curved pattern and tended to be superimposed. The curved structures could result in a large static disorder of the W–W distance. Such curved sites in the WS_2 crystallites probably cause the formations of more sulfur vacancy sites, and more catalytically active sites.

3.2.6. XPS analysis

The W4f spectra of sulfided catalysts are shown in Fig. 9. After deconvolution, a doublet peak appeared at 34.4 and 32.5 eV, which were the typical characteristics of tungsten sulfide (WS_2) [13]. The degree of sulfidation of W species was determined from the curve fitting (Fig. 9), based on the equation of $W_{sulfide}/W_{total} = W_{sulfide}/(W_{oxide} + W_{sulfide})$. The results showed that the sulfidation degrees (50% and 55%, respectively) of W species in both NiW/Al_2O_3–MB and NiW/TiO_2–Al_2O_3–MB were much higher than that of NiW/Al_2O_3 (42%), which might be due to the difference in the interactions of W species with the support in different catalysts. High sulfidation degree would lead to higher HDS activity.

3.2.7. HDS activity evaluation

The diesel HDS results are shown in Fig. 10 and Table 5. The FCC diesel feed used in this experiment contained various kinds of sulfur compounds, mainly including BT, alkyl-substituted BT, DBT and alkyl-substituted DBT (as shown in Table 5), and the high sulfur content of feed reached to 1300 ppm. Compared with NiW/Al_2O_3 (97.5%), the MB-containing catalysts exhibited higher HDS conversion (as shown in Fig. 10), and the HDS conversion of NiW/Al_2O_3–MB and NiW/TiO_2–Al_2O_3–MB increased by 1.2% and 1.8%, respectively, For comparison, the sample containing traditional zeolite beta was also included. Compared with NiW/Al_2O_3, it is interesting that the HDS conversion of NiW/TiO_2–Al_2O_3–B containing traditional zeolite beta increased by 0.8 and it was lower than those of NiW/Al_2O_3–MB and NiW/TiO_2–Al_2O_3–MB catalysts.

From Table 5, the percentages of alkyl-BT and alkyl-DBT over total sulfur contents in feedstock were 56.9 and 36.7 wt%, respectively. The sulfur distribution in product also indicated that alkyl-substituted DBT compounds were the most difficult com-

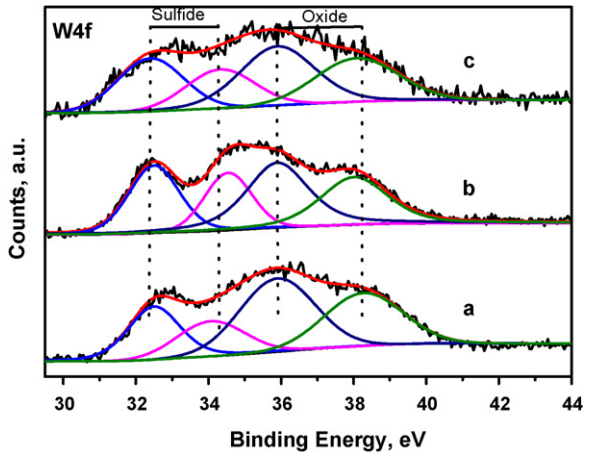

Fig. 9. XPS W4f spectra of sulfided (a) NiW/Al_2O_3, (b) NiW/Al_2O_3–MB and (c) NiW/TiO_2–Al_2O_3–MB.

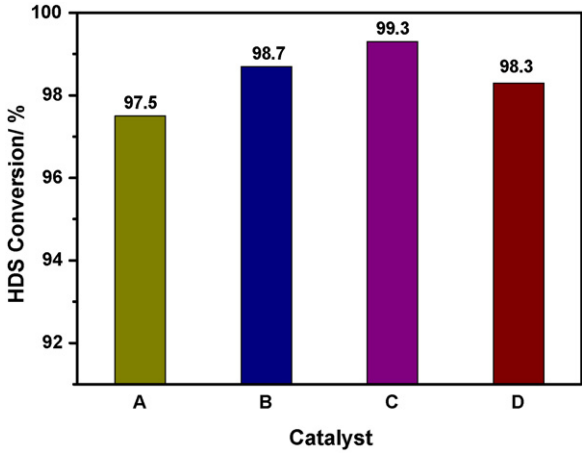

Fig. 10. The HDS conversions of NiW catalysts (A) NiW/Al_2O_3, (B) NiW/Al_2O_3–MB, (C) NiW/TiO_2–Al_2O_3–MB and (D) NiW/TiO_2–Al_2O_3–B.

Table 5
The sulfur compounds in feed and in products over NiW catalysts after HDS.

Sulfur compound	Feed (ppm)	NiW/Al_2O_3 (ppm)	NiW/Al_2O_3–MB (ppm)	NiW/TiO_2–Al_2O_3–MB (ppm)	NiW/TiO_2–Al_2O_3–B (ppm)
BT	28.8	–	–	–	
C1-BT	145.2	–	–	–	
C2-BT	249.5	–	–	–	
≥C3-BT	345.2	–	–	–	
DBT	53.8	–	–	–	
C1-DBT	135.1	–	–	–	
C2-DBT	146.2	11.8	8.0	1.9	
≥C3-DBT	196.3	20.4	8.7	6.8	
Total	1300	32.2	16.7	8.7	21.9

pounds to be removed from the diesel. NiW/Al_2O_3–MB and NiW/TiO_2–Al_2O_3–MB exhibited higher HDS conversions of alkyl-substituted DBT than NiW/Al_2O_3.

From those results above, it could be concluded that the addition of MB and/or TiO_2 to the catalyst support led to a higher HDS catalytic activity than the conventional alumina-supported counterpart. The increase in HDS activity was due to the enhanced hydrogenation activity and increased B acidity proportion caused by the incorporation of MB and TiO_2.

The enhanced hydrogenation activity was likely associated with the particle sizes of WS_2 active sites. The single-slab structure (usually called type-I WS_2) interacted strongly with the support, whereas the multiple-slab form (called type-II WS_2) had weak interaction with the support and exhibited greater hydrogenation activity [29,30]. MB-containing catalysts showed much higher WS_2 slab sizes and layers than those of NiW/Al_2O_3. Multilayered WS_2 slabs provided a higher density of multivacancies compared with single-layered slabs. Vradman et al. also concluded that the high stacking number of WS_2 slabs could enhance the HYD activity [31].

After the addition of MB and TiO_2 to Al_2O_3 support, the interaction of WS_2 with the support of Al_2O_3 was weakened, the sulfidation degree of W and the WS_2 slab sizes on the catalysts increased significantly, which could lead to an increase of hydrogenation performance of the catalysts. In MB-containing catalysts, NiW/TiO_2–Al_2O_3–MB showed shorter WS_2 slab sizes and lower layers than those of NiW/Al_2O_3–MB, while NiW/TiO_2–Al_2O_3–MB exhibited higher HDS activity than that of NiW/Al_2O_3–MB. Obviously, there existed a compromise between WS_2 slab sizes and stacking degree for achieving the optimal catalyst performance. Moreover, the increase in hydrogenation performance of the NiW/TiO_2–Al_2O_3–MB catalysts also could be due to the electronic promotion effect of TiO_2. Ti^{3+} centers formed under HDS reaction conditions can transfer electronic charge to the sulfided W active phases making more easy the formation of coordinatively unsaturated sites or sulfur vacancies, thus the HDS activity could be greatly promoted [32].

The acidity is likely another important factor to improve HDS activities of MB-containing catalysts. The addition of MB led to an increase of the proportion of B acid or the ratio of B/L. In addition, the incorporation of TiO_2 further modulated the ratios of B/L. Therefore, the acid types, i.e., the ratio of B/L and acid strength seemingly played a key role in promoting HDS activities of the catalysts. It could be concluded that suitable ratio of B/L was favorable for achieving high HDS conversions of diesel.

4. Conclusions

A new type of zeolite beta with multi-pore system, MB, was successfully synthesized from kaolin material in present work, and the new type of materials in FCC diesel hydrodesulfurization showed good catalytic performance.

The addition of MB zeolite and/or TiO_2 tuned the B/L acid ratio, reduced the interaction between W and the support, and increased the sulfidation extent of W. The incorporation of MB made the WS_2 slabs grow larger, stacking degree become higher and formed type-II conformation which had greater hydrogenation activity. NiW/TiO_2–Al_2O_3–MB exhibited the highest HDS efficiency of 99.3%. The addition of Ti and H-MB greatly improved the HDS activities of FCC diesel.

Acknowledgments

The authors acknowledge the financial supports from 973 National Basic Research Program of China (No. 2004CB217806), Natural Science Foundation of China (No. 20876173, No. 20833011 and No. 20773163).

References

[1] T.C. Ho, Catal. Today 98 (2004) 3.
[2] E.J.M. Hensen, P.J. Kooyman, Y. van der Meer, A.M. van der Kraan, V.H.J. de Beer, J.A.R. van Veen, R.A. van Santen, J. Catal. 199 (2001) 224.
[3] J.R. Grzechowiak, J. Rynkowski, I. Wereszczako-Zielinska, Catal. Today 65 (2001) 225.
[4] P. Rayo, J. Ancheyta, J. Ramírez, A. Gutiérrez-Alejandre, Catal. Today 98 (2004) 171.
[5] J.R. Grzechowiak, I. Wereszczako-Zielińska, K. Mrozińska, Catal. Today 119 (2007) 23.
[6] G. Pérot, Catal. Today 86 (2003) 111.
[7] F. Bataille, J. Lemberton, P. Michaud, G. Pérot, M. Vrinat, M. Lemaire, E. Schulz, M. Breysse, S. Kasztelan, J. Catal. 191 (2000) 409.
[8] F. Bataille, J.L. Lemberton, G. Pérot, P. Leyrit, T. Cseri, N. Marchal, S. Kasztelan, Appl. Catal. A 220 (2001) 191.
[9] T. Isoda, S. Nagao, X. Ma, Y. Korai, I. Mochida, Energy Fuels 10 (1996) 1078.
[10] C. Song, Catal. Today 86 (2003) 211.
[11] K. Choi, N. Kunisada, Y. Korai, I. Mochida, K. Nakano, Catal. Today 86 (2003) 277.
[12] N. Kunisada, K. Choi, Y. Korai, I. Mochida, K. Nakano, Appl. Catal. A 276 (2004) 51.
[13] S. Bendezú, R. Cid, J.L.G. Fierro, A. López Agudo, Appl. Catal. A 197 (2000) 47.
[14] A. Corma, V. Fornés, J.B. Montón, A.V. Orchillés, J. Catal. 107 (1987) 288.
[15] M.A. Ali, T. Tatsumi, T. Masuda, Appl. Catal. A 233 (2002) 77.
[16] A. Hassan, S. Ahmed, M.A. Ali, H. Hamid, T. Inui, Appl. Catal. A 220 (2001) 59.
[17] L. Ding, Y. Zheng, Z. Zhang, Z. Ring, J. Chen, J. Catal. 241 (2006) 435.
[18] G. Wan, A. Duan, Y. Zhang, Z. Zhao, D. Zhang, Z. Gao, G. Jiang, Prepr. Pap.—Am. Chem. Soc., Div. Pet. Chem. 53 (2008) 203.
[19] D.C. Vermaire, P.C. Van Berge, J. Catal. 116 (1989) 309.
[20] L. Karakonstantis, H. Matralis, C. Kordulis, A. Lycourghiotis, J. Catal. 162 (1996) 306.
[21] D.G. Barton, S.L. Soled, G.D. Meitzner, G.A. Fuentes, E. Iglesia, J. Catal. 181 (1999) 57.
[22] B. Sheffer, P. Molhoek, J.A. Moulijn, Appl. Catal. 46 (1989) 11.
[23] J. Ramírez, A. Gutiérrez-Alejandre, Catal. Today 43 (1998) 123.
[24] D. Solís, A. López Agudo, J. Ramírez, T. Klimova, Catal. Today 116 (2006) 469.
[25] G. Poncelet, M.L. Dubru, J. Catal. 52 (1978) 321.
[26] J.S. Lee, M. Boudart, Catal. Lett. 20 (1993) 97.
[27] C. Glasson, C. Geantet, M. Lacroix, F. Labruyere, P. Dufresne, J. Catal. 212 (2002) 76.
[28] H.R. Reinhoudt, A.D. van Langeveld, P.J. Kooyman, R.M. Stockmann, R. Prins, H.W. Zandbergen, J.A. Moulijn, J. Catal. 179 (1998) 443.
[29] H. Topsøe, B.S. Clausen, N.-Y. Topsøe, P. Zeathen, Stud. Surf. Sci. Catal. 53 (1989) 77.
[30] H. Topsøe, B.S. Clausen, Appl. Catal. 25 (1986) 273.
[31] L. Vradman, M.V. Landau, M. Herskowitz, Fuel 82 (2003) 633.
[32] J. Ramírez, G. Macías, L. Cedeño, A. Gutiérrez-Alejandre, R. Cuevas, P. Castillo, Catal. Today 98 (2004) 19.